SIMULATION AND EXPERIMENT ON THE PROCESS OF CASTOR SHELLING BASED ON DISCRETE ELEMENT METHOD

/

可调式蓖麻脱壳机脱壳过程离散元分析与试验

Junming HOU, Zhaotan REN, Hongjie ZHU, Zhi RENDE, Wei WANG
Shenyang Agricultural University, College of Engineering / China;
Tel: +86024-88487116; E-mail: junming_hou@163.com
DOI: https://doi.org/10.35633/inmateh-70-04

Keywords: *castor, stress analysis, experiment, DEM, design optimization*

ABSTRACT

Castor is one of the important oil crop, the shelling process of which directly affects the quality of castor seeds. In the process of shelling, the shelling force of castor is an important index to study its damage. The castor capsule model was established and the shelling test machine was established based on the discrete element method. Then the extrusion law of castor capsule during shelling was analyzed. The shelling process is divided into three stages, which are the Initial stage*,* stable shelling stage *and the* final stage*. The force law of shelling process is analyzed. The results show that with the increase of rotating speed, the maximum force decreases from 68.78 to 68.10 N, the maximum speed increases from 8.92 to 12.99 m/s, the force of inner drum increases from 509.34 to 533.14 N, and then decreases to 456.15 N. The shelling increases from 91.23% to 91.28%, and then decreases to 88.89%. With the increase of filling amount, the maximum force increases from 55.86 to 76.93 N, the maximum speed decreases from 12.99 to 10.86 m/s, the force of inner drum increases from 338.58 to 603.364 N, and the shelling rate changes from 91% to 90.05%. This study can provide theoretical support for the design of castor shelling machine.*

摘要

蓖麻是重要的油料作物，其脱壳过程直接影响蓖麻种子的质量。在脱壳过程中，蓖麻的受力是研究其损伤的重要指标。本研究基于离散元方法，建立了蓖麻蒴果模型并搭建了脱壳试验台。分析蓖麻蒴果在脱壳过程中的挤压规律。该过程分为三个阶段，即开始阶段、稳定阶段和结束阶段。分析了三个阶段的脱壳过程的应力规律。结果表明，随着转速的增加，最大受力从 68.78 N 降至 68.10 N，最大转速从 8.92 m/s 升至 12.99 m/s，内筒应力从 509.34 N 升至 533.14 N，然后降至 456.15 N，脱壳率从 91.23%升至 91.28%，然后降至 88.89%。随着装填量的增加，最大压力从 55.86 N 增加到 76.93 N，最大速度从 12.99 m/s 降低到 10.86 m/s，内筒应力从 338.58 N 增加到 603.364 N，脱壳率从 91%变为 90.05%。本研究可为蓖麻脱壳机的设计提供理论支持。

INTRODUCTION

Castor is one of the ten oil crops in the world. Castor oil extracted from seeds has a high viscosity, ignition point and low freezing point, which is one of the advanced lubricating oils for trains, high-speed lathes, and aerospace (*Huang et al., 2013; Liu et al., 2015*). Shelling is the first step of castor oil processing, which directly affects its quality. The force law of castor is a vital index to affect the damage of castor capsule during the process of shelling.

Güner et al., (2003), determined the fracture force and fracture energy required for hazelnut shell breaking, which provided a reference for the design of hazelnut sheller. The anisotropic behavior of hazelnut was analyzed with numerical simulation (*Delprete et al., 2014*). The significant data of mechanical properties was obtained, which can provide a reference for the design of shelling machine. The effect and shelling mechanism of rubber materials on the shelling performance of grain sheller was studied (*Baker et al., 2012*). The results show that the shear force is the main factor affecting the shelling rate. The mechanical behavior of collision between rice grain and the key parts of shelling machine was studied (*Zhao et al., 2013*). The results show that the difference of normal contact force increased with the increase of particle size ratio. The geometric model and stress model for ginkgo biloba were established, which can analyze the stress based on the finite element method (*Wang et al., 2003*).

The best direction and mode of force application were found, which provides a theoretical basis for the development of shelling equipment. The shelling method of ginkgo fruit was determined, and the force of ginkgo fruit in extrusion working area was analyzed (*Pan et al., 2019*). The finite element model of chestnut shell breaking was established in vacuum. The results show that the wet stress is the main factor of chestnut shell breaking in vacuum (*Yuan et al., 2011*). The mechanical behavior of *Jatropha curcas L.* seeds under compression was studied. The results showed that the stamping speed has a great influence on deformation, deformation energy and oil yield (*Kabutey et al., 2013*). Wang studied the mechanical properties of kenaf capsule (*Wang et al., 2015*). The results showed that the capsule began to break from the middle near the top and then produced cracks to make the seeds come out of the capsule. The nonlinear relationship between water content, loading speed, transverse diameter ratio and shell breaking force of walnut was established, which provided the law of shell breaking conditions and crack variation characteristics (*Zhang et al., 2014*). Liu et al. (*2016*) analyzed the stiffness of walnut shell by mechanical theory of elasticity. The dynamic response of different drop height to the impact of potato rigid plate was supervised (*Gao et al., 2018*). The results show that the maximum impact force and the maximum deformation are positively correlated with the drop height. The mechanical behavior of *Jatropha curcas L.* seeds was studied at different pressing vessel diameters and seed pressing heights under compression loading (*Herak et al., 2013*). The mathematical models can provide the basis for the development of further models. The mechanical properties of the sides and middle parts of the film were enhanced to improve the recovery efficiency of residual film (*Hu et al. 2017*). The results suggested that the film was of tensile strength after its mechanical properties have been reinforced. The force and rate of shelling removal of the inner drum were analyzed (*Hou et al., 2020*). The results provided theoretical support for the design of the castor shelling machine. The minimum fall height of potatoes falling onto steel sheets, steel rods and rubber-steel rods causing unallowable damage to potatoes was studied (*Rady et al., 2015*). The results showed that steel sheet and steel rods resulted in higher bruise volume values compared to the coated steel rods. The design of the seed metering device was optimized (*Shi et al., 2020*). The result showed that the optimized seed plate had a better performance at high speed and vibration conditions. The collision recovery coefficient of soybean seed contact with seed plate, seed wheel and organic glass was determined (*Zhang et al., 2017*). The results showed that the collision recovery coefficients were 0.561, 0.518 and 0.472, respectively.

The critical forces of walnut, the vital forces of shell breaking, and the conditions of crack propagation after fracture were obtained. Considering the related studies, progress has been made in the study of the mechanical law of agricultural materials shelling. However, the process of shelling on agricultural particles based on Discrete Element Method (DEM) has not been studied in detail deeply. Especially, the force parameters of particles in the shelling process were not discussed.

In the study, the model of castor was established based on DEM. The law of force extrusion in the process of shelling was analyzed. The shelling process is divided into three stages, which are the beginning shelling stage, stable stage, and the ending stage. The shelling process and force law of the three stages were analyzed.

MATERIALS AND METHODS

Establishment of castor model

The castor capsule bond model was established. The relationship between the force and displacement of particles in each contact motion was described. Its three axis dimensions are 15.00 mm in length, 14.50 mm in width, and 16.00 mm in height. The contact of particles, center of the area, line between the center point of two particles, and the center point were established.

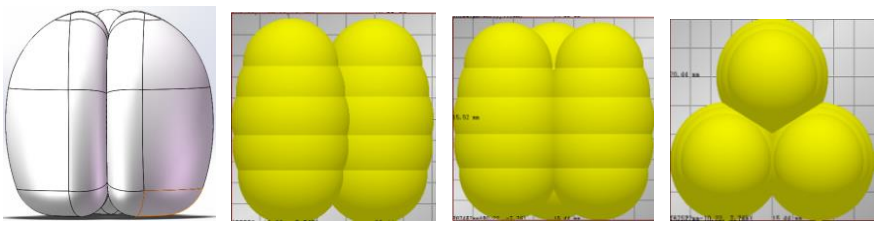

(a) Three-dimensional map (b) Direction X (c) Direction Y (d) Direction Z

Fig. 1 - 3 DEM model of castor fruit

Division of shelling stage for castor capsule

The variety of TongBi No.7 castor was selected as the test material. The replacement effect occurs at 0.395 s during the simulation. At 1.5 s, the particles fell into the shelling drum and began to shell. Fig. 2 shows the process of castor shelling.

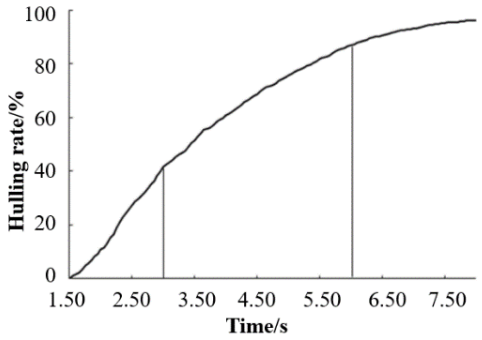

Fig. 2 - The process of castor shelling

It can be drawn that the shelling rate rose rapidly from 1.5 s to 3 s. It ran stably from 1.5 s to 6 s, and ran gently from 6 s to 8 s. It continued to rise from 1.6 s to 6 s, then it ran smoothly from 6 s to 8 s. Therefore, the shelling process was divided into three stages which are the initial, stable, and ending shelling stages. The three stage curve fitting equation and correlation coefficient are shown in Table 1.

Table 1

Regression equation of undamaged bond

Shelling distance process	Fitting equations	The correlation coefficient
Initial stage	Y=1.44X-3.86	0.9939
Stable shelling stage	Y=0.75X+43.66	0.9878
Final stage	Y=0.23X+87.78	0.9630

It can be drawn that the shelling efficiency decreased continuously in the process of shelling. Therefore, the shelling efficiency shows a downward trend. The correlation coefficients of the fitting equation are all close to 1.0. Table 2 shows the division of shelling stages.

Table 2

Division of shelling stages

Shelling distance stage	Feeding	Initial stage	Stable shelling	The end of the shelling
Period of time/s	0~1.5	1.5~3	3~6	6~8

Simulation of castor capsule at the initial stage

The relationship between average velocity and maximum particle force is shown in Fig. 3. It can be drawn that when the average speed of particles reached 1.81 m/s, the maximum force of particles reached a maximum value of 48.86 N. When the average particle velocity reached 1.77 m/s, the maximum particle force reached the minimum value of 10.04 N. When the average speed of particles was from 1.57 m/s to 1.83 m/s, the maximum force of particles fluctuated greatly, and the fluctuation frequency was small. When the average velocity of particles changed from 1.83 m/s to 1.95 m/s, the maximum force fluctuation of particles was low. Because the particles entered the shelling part in a short time, the force changed significantly.

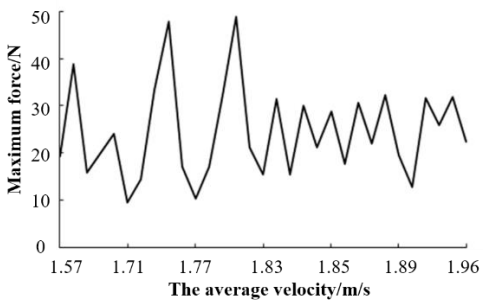

Fig. 3 - Relationship of average velocity and maximum force

The force exerted by the particle groups on the shelling model is shown in Fig.4. It can be seen that with the progress of the shelling process, the force produced by the external drum of particles changes smoothly, reaching the maximum value of 101.53 N at 1.75 s.

The average force at the beginning of the shelling stage was 47.28 N. The force exerted by particles on the inner drum fluctuated greatly, reaching a maximum value of 245.09 N at 2.75 s. The average force was 141.73 N in this stage. At this stage, the particles fall into the shell chamber from the inlet. Comparing the force of particles on the inner with outer drums, it can be seen that the force of the inner drum is higher than the outer drum at the same time. Therefore, the inner drum performs the main shelling work at this stage. The force fluctuation range of the inner drum is extensive, so the shelling effect at this stage is mainly the collision between the particles and the drum.

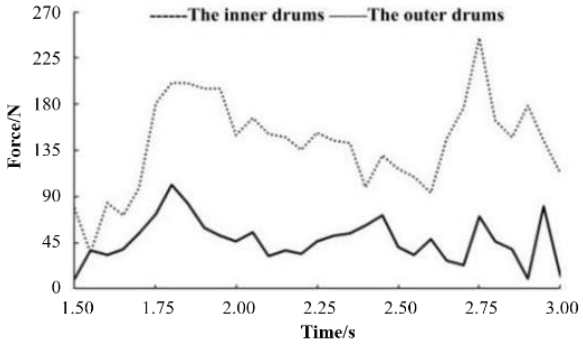

Fig. 4 – Force of particle group to shelling model

The average and tangential force among particles is shown in Fig.5. According to Fig.5 (a), in the X-axis direction, when the average velocity of particle reached 1.81 m/s, the maximum force among particles reached 23.66 N. When the average velocity of particle reached 1.57 m/s, the maximum force among particles reached 5.75 N. When the average particle velocity reached 1.71 m/s, the maximum force among particles reached 6.29 N. When the average particle velocity reached 1.57 m/s, the maximum force among particles reached 4.34 N.

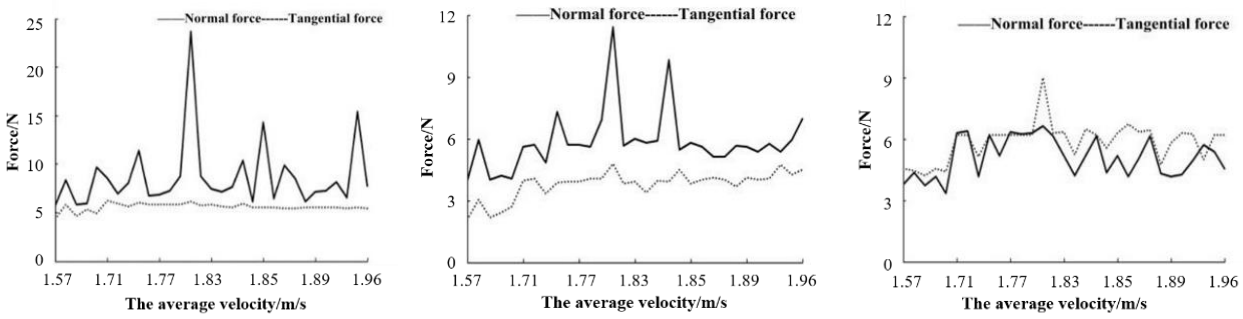

(a)X direction (b)Y direction (c)Z direction

Fig. 5 - Contact forces between particles

Fig.5 (b) shows the results in the Y-axis direction. When the average velocity of particle reached 1.81 m/s, the maximum force among particles reached 11.45 N. When the average speed of particles reached 1.57 m/s, the maximum force among particles reached the minimum value, which is 3.99 N. When the average particle velocity reached 1.81 m/s, the maximum tangential force among particles reached 4.82 N. When the average speed of particles reached 1.57 m/s, the maximum force among particles reached the minimum value, which is 2.06 N.

Fig.5 (c) shows the results in the Z-axis direction. When the average particle velocity reached 1.81 m/s, the maximum normal force among particles reached 6.62 N. When the average velocity of particles reached 1.70 m/s, the maximum force among particles reached the minimum value, which is 3.36 N. When the average particle velocity reached 1.81 m/s, the maximum tangential force among particles reached 9.03 N. When the average speed of particles reached 1.65 m/s, the maximum force among particles reached the minimum value, which is 4.22 N. The results show that the inner and outer rollers jointly provide the shelling effect, and the frequency difference of force fluctuations caused by particles on the inner and outer rollers is small.

Simulation of stable shelling stage

The relationship between average velocity and maximum particle force is shown in Fig. 6. It can be drawn that in the stable shelling stage, when the average velocity of particles reached 1.77 m/s, the maximum force of particles reached a maximum value of 41.39 N.

When the average speed of particles reached 1.51 m/s, the maximum force of particles reached the minimum value, which is 6.98 N. When the average velocity of particles was between 1.44 m/s and 1.59 m/s, the maximum force of particles fluctuates greatly.

When the average velocity of particles was from 1.59 m/s to 1.76 m/s, the maximum force fluctuation of particles was low. When the average velocity of particles was from 1.76 m/s to 1.84 m/s, the maximum force of particles fluctuated greatly. The reason is that particles are uniformly distributed in the inner part of the shelling chamber, and the inner and outer rollers act together to remove the shell.

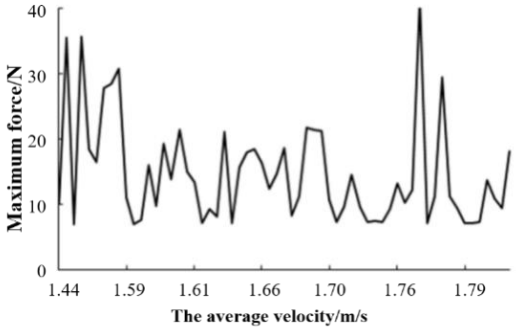

Fig. 6 - Relationship of average velocity and maximum force

The force of particle group in the shelling process is shown in Fig. 7. It can be drawn that the force generated by the particles in the external drum. It presented a downward trend with the progress of the shelling process. The maximum value is 74.39 N when the time is 3.30 s. The average value was 23.87 N in this stage. The force exerted by particles on the inner drum showed a downward trend, reaching a maximum value of 133.80 N at 3.10 s. The average value was 26.79 N in this stage. By comparing the force on the inner and outer drum, it can be drawn that the particles evenly distributed in the interior of the shelling region. Therefore, the outer and inner drum worked together to break the shell in this stage. The particles were impacted, squeezed and rubbed together with the drums.

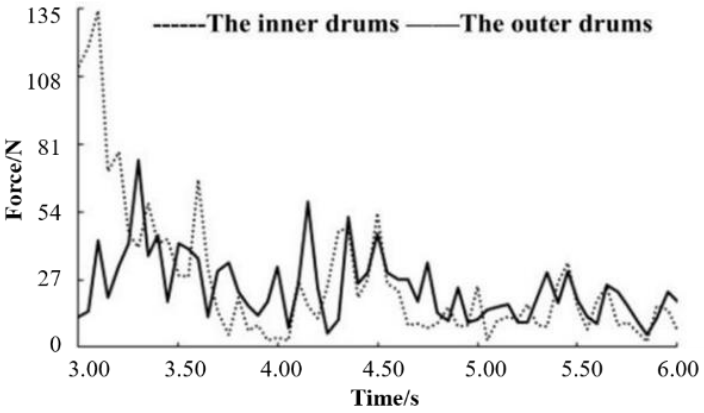

Fig. 7 - Force of particle group in the shelling process

The law of the normal and tangential forces among particles is shown in Fig.8. It can be seen from Fig.8(a) that when the average particle velocity reached 1.67 m/s, the maximum force among particles reached 12.55 N in the X-axis direction. When the average particle velocity reached 1.57 m/s, the maximum normal force among particles reached to the minimum value, which was 5.75 N. When the average particle velocity reached 1.73 m/s, the maximum tangential force among particles reached 6.97 N. When the average speed of particles reached 1.96 m/s, the maximum reasonable force among particles reached the minimum value, which was 5.50 N.

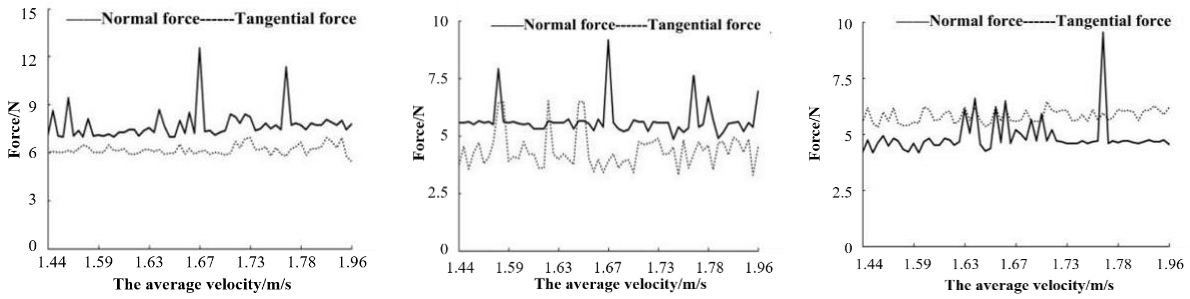

(a) X direction (b) Y direction (c) Z direction

Fig. 8 - Contact force between particles

Fig.8 (b) shows that when the average particle velocity reached 1.67 m/s, the maximum reasonable force between particles reached 9.16 N in the Y-axis direction. When the average particle velocity reached 1.75 m/s, the maximum reasonable force among particles reached the minimum value, which was 4.88 N. When the average particle velocity reached 1.61 m/s, the maximum tangential force among particles reached 6.51 N. When the average speed of particles reached 1.76 m/s, the maximum reasonable force among particles reached the minimum value, which was 3.31 N.

Fig.8(c) shows that when the average particle velocity reached 1.77 m/s, the maximum normal force among particles reached 9.54 N in the Z-axis direction. When the average speed of particles reached 1.51 m/s, the maximum normal force among particles reached the minimum value, which was 4.16 N. When the average particle velocity reached 1.70 m/s, the maximum tangential force among particles reached 6.44 N. When the average speed of particles reached 1.52 m/s, the maximum reasonable force between particles reached the minimum value, which was 5.30 N. The frequency of force fluctuations generated by particles on the external drum is high. At this stage, the collision between the capsules and their forces on the shelling parts cause them to break.

Simulation of final shelling stage

The relationship between average velocity and maximum particle force is shown in Fig.9.

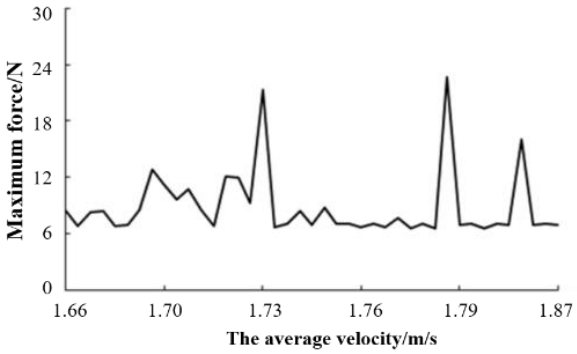

Fig. 9 - Variation of average velocity with maximum force

It can be drawn that when the average particle velocity reached 1.79 m/s, the maximum particle force reached a maximum value of 22.59 N. When the average particle velocity reached 1.78 m/s, the maximum particle force reached the minimum value of 6.56 N. In this stage, with the increase of average speed, the maximum force fluctuation of particles is relatively stable. The collision between the capsules and their forces on the shelling parts cause them to break.

The force exerted by particles group on the shelling model is shown is Fig.10. It can be drawn that the force generated by particles in the external drum. It decreased with process of shelling, reaching a maximum value of 25.87 N at 6.75 s. The force exerted by particles on the inner drum decreased with the prolonging of the shelling process when it reached a maximum value of 21.64 N at 7.80 s. By comparing the force of particles on the internal and external drums, the inner and outer drums provided the shelling effect in this stage. Moreover, the force fluctuation of particles on the inner and outer drums was small. Therefore, the outer and inner drums worked together to complete the shelling in this stage.

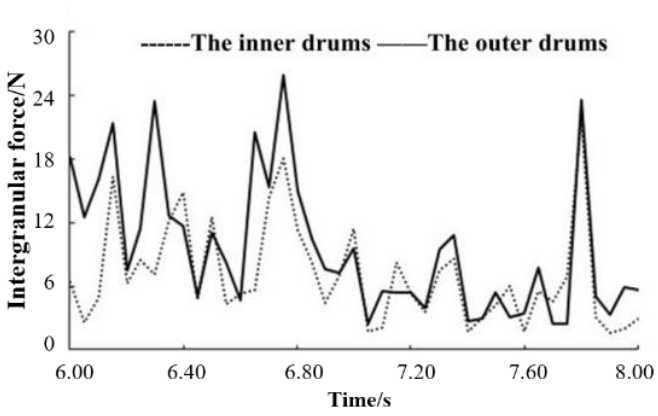

Fig. 10 - Force of particle group on the shelling model

To analyze the interaction among particles during the shelling process, the average and tangential forces of the interaction among particles are shown in Fig.11.

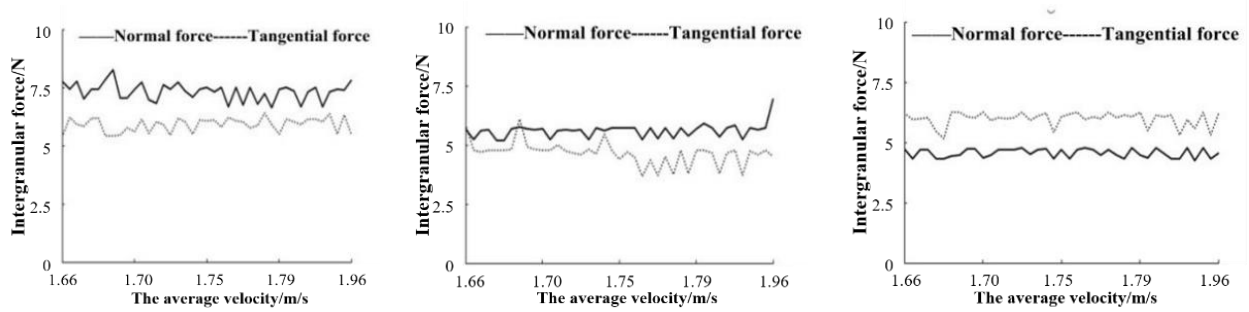

(a) X direction (b) Y direction (c) Z direction

Fig. 11 - Force of the particles

According to Fig.11 (a), when the average particle velocity reached 1.70 m/s, the maximum force among particles reached 8.25 N in the X-axis direction. When the average speed of particles reached 1.78 m/s, the maximum force among particles reached the minimum value, which was 6.65 N. When the average particle velocity reached 1.78 m/s, the maximum tangential force among particles reached 6.40 N. When the average speed of particles reached 1.66 m/s, the maximum force among particles reached the minimum value, which was 5.41 N.

According to Fig.11 (b), when the average particle velocity reached 1.96 m/s, the maximum force between particles reached 6.95 N in the Y-axis direction. When the average particle velocity reached 1.69 m/s, the maximum reasonable force among particles reached the minimum value, which was 5.19 N. When the average speed of particles reached 1.70 m/s, the maximum tangential force among particles reached 6.09 N. When the average velocity of particles reached 1.76 m/s, the maximum reasonable force among particles reached the minimum value, which was 3.70 N.

When the average speed of particles reached 1.76 m/s, the maximum tangential force among particles reached 6.27 N. When the average particle velocity reached 1.69 m/s, the maximum force among particles reached the minimum value, which was 5.15 N.

The extrusion among the particles and the drums worked to complete the shelling. So, the force among the particles changes in the way.

Analysis of transition phase and key grid

Considering the continuity and integrity of the process, there is a transition stage among the three stages. The maximum force, particle normal force, and triaxial displacement of the particles are mostly between the two period of 2.75-3.25 s and 5.75-6.25 s. Table 3 shows the size comparison of the results of particles at the time of 2.75 s, 3.25 s, 5.75 s, and 6.25 s.

Table 3

Statistics of the result size at each moment of the particles

Time	Maximum force	Interparticle normal resultant force	Interparticle tangential resultant force	Displacement
[s]	[N]	[N]	[N]	[mm]
2.75	48.86	27.11	11.94	885.54
3.25	26.01	10.21	8.83	944.95
5.75	9.36	10.84	10.39	1255.75
6.25	7.61	7.12	7.63	1409.6

Fig.12 shows the critical state of particles. The result shows that the distribution grid in the process of shelling.

It showed a trend of growth in the interval from 1.5 s to 2.75 s. The particles number was stable from 2.75 s to 3.25 s. The large number of particles distribution was from 3.25 s to 5.75 s. When the time was between 5.75 s and 6.25 s, the amount of particles was on the decline. Fig.11(b) shows the maximum force in the grid. It can be drawn that the maximum force decreased with the continuation of the shelling process and reached zero gradually with the continuous discharge of particles. Fig.11 (c) shows the maximum velocity of particles in the grid. The maximum speed decreased with the continuation of the shelling process and reached to zero gradually with the continuous discharge of particles.

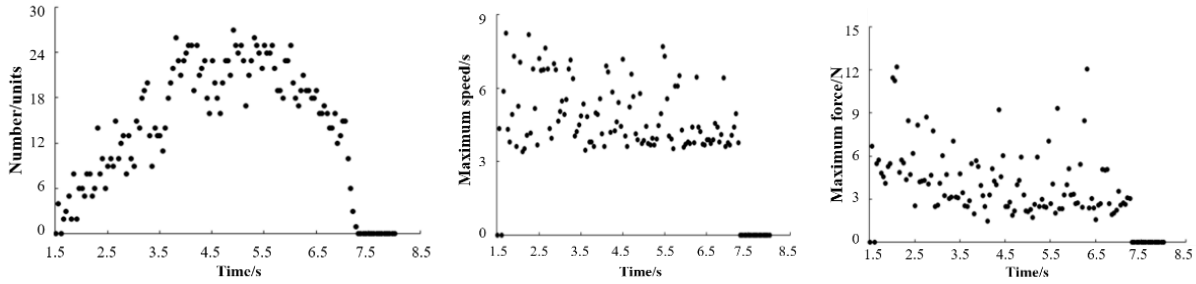

(a) **(b)** **(c)**

Fig. 12 - Critical grid state of particles

Test methods and instruments

The speed of the inner drum, the distance of shell removal and the filling amount were the test factors, while the rate of shell removal, damage rate and productivity were the test indicators. The speed of the inner drum can be changed through the frequency converter, the position of the outer drum was adjusted to change the shell distance, and the amount of feed is adapted to fit the filling amount. The high speed camera was directed towards the observation window, and recorded the status of particles in the drum within 1.5 s to 8 s after feeding through high-speed photography (*Hou et al., 2020)*.

Fig. 13 - Castor Shelling Test Bed

1. Host; 2. Motor; 3. Light source; 4. Adjustment hole; 5. Frequency converter; 6. Adjustment arm; 7. Shelling drum; 8. Feeding hopper; 9. Observation window; 10. Frame; 11. Camera

The experimental material was castor capsule Tongbi No.11, which was dried in Tongliao Academy of Agricultural Sciences, Inner Mongolia. The test equipment includes castor capsule shelling machine, Shuangjie electronic scale (TC-60K) (maximum weighing 60 kg, accuracy 10.0 g). The shelling machine equipment is shown in Fig.13.

RESULTS

Shelling machine design

Based on the parameter setting of the simulation shelling model, the shelling machine was designed. Through changes in the amount of drum rotating speed, the shelling distance and filling amount were taken as the factors, damage rate and productivity were as an index. The schematic diagram of the shelling machine is shown in Fig.14.

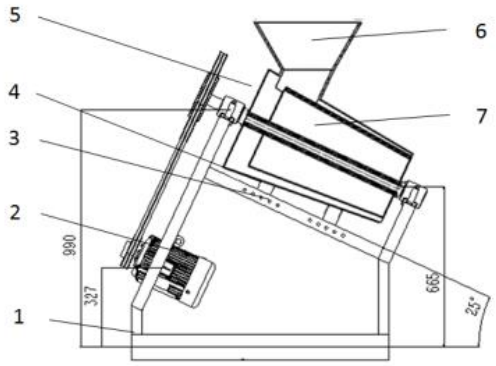

Fig. 14 - Schematic diagram of complete machine

1. Motor; 2. Base frame; 3. Adjustment hole; 4. Adjustment arm; 5. Outer drum; 6. Feed hopper; 7. Inner drum

Analysis of test results

The rotating speed of the inner drum, the shelling distance, and the filling amount are the test factors, and the shelling rate, damage rate, and productivity are the test indicators. The test bench test is conducted. The level table is shown in Table 4.

Table4

Test Factor level

Level	Speed rpm	Shelling distance mm	Filling amount %
-1	250	5	30
0	300	6	40
1	350	7	50

The analysis of variance of shell removal rate is shown in Table 5. The test statistic value *F* represents inter group differences. The significance level is *P* value. It can be drawn that the rotation speed, shelling distance and filling amount have an extremely significant influence on the rate of shelling, among which the shelling distance has the most considerable impact, followed by rotation speed. The filling amount was the smallest.

Table 5

Variance analysis results

Sources of variance	Square sum	Freedom	Mean square	*F* value	*P* value
A	18.29	2	9.15	134.14	<0.01
B	27.59	2	13.79	202.21	<0.01
C	12.14	2	6.07	89.01	<0.05
Error	0.14	2	0.07		
Summation	58.17	8			

Table 6 is the variance analysis of damage rate. It can be seen that the speed and the shelling distance had an extremely significant influence on the damage rate.

Table 6

Variance analysis results

Sources of variance	Square sum	Freedom	Mean square	*F* value	*P* value
A	0.13	2	0.06	134.23	<0.01
B	0.13	2	0.07	139.00	<0.01
C	0.04	2	0.02	43.53	<0.05
Error	9.56×10^{-4}	2	4.78×10^{-4}		
Summation	0.30	8			

Furthermore, the impact of the shelling distance was greater than the speed, and the filling quantity had a considerable influence on the damage rate. Table 7 shows the productivity variance analysis.

Table 7

Variance analysis results

Sources of variance	Square sum	Freedom	Mean square	*F* value	*P* value
A	10672.16	2	5336.08	239.44	<0.01
B	4698.14	2	2349.07	105.41	<0.01
C	424.24	2	212.12	9.52	<0.1
Error	44.57	2	22.29		
Summation	15839.11	8	7919.55		

It can be drawn that the speed and the shelling distance had an extremely significant impact on productivity. The speed had a greater impact than the shelling distance, and the filling amount has a considerable effect on productivity.

Comparison of shelling rate

The significance order of each factor obtained by simulation was the shelling distance, rotation speed and filling amount. The significance order of each factor obtained by experiment was the shelling distance, rotation speed and filling amount. The optimal combination obtained by the simulation was 350.0 r/min, the shelling distance was 5 mm, and the filling amount was 40.0%. The optimal combination obtained by the test was 350.0 r/min, the shelling distance was 5.0 mm, and the filling amount was 30.0%. The speed and the shelling distance were incredibly significant factors, and the filling amount was a substantial factor, which is within a reasonable range.

CONCLUSIONS

(1) The shelling distance and the filling amount have a significant impact on the force of the inner drum, while the rotating speed has no significant impact on the force of the inner drum. With the increase of the shelling distance and the filling amount, the force of the inner drum increased.

(2) The shelling process is divided into three stages. At the initial stage, the maximum force of the particle is generated, which is 48.86 N. The main shelling form is collision. At the stable stage, the force fluctuation frequency of the particle is the highest. The shelling work is completed by the inner and outer drum together. At the final stage, the force fluctuation frequency of the particle on the inner and outer drum is less different. The inner and outer drum work together to complete the shelling. The main form of shelling is extrusion and rubbing.

(3) The optimized within roller cone angle is 4.5°, drum length is 605.0 mm with the highest for shelling rate under the conditions of size parameter adjustment. The rate of shell removal is 96.42% when the size parameters are applied for simulation. There was a difference of 0.39% from the fitting value.

(4) The simulation model is verified on test bed. The shelling rate was significantly affected by the rotation speed, shelling distance and filling amount. The shelling damage rate was significantly affected by the rotation speed. By comparing the shelling rate, it can be seen that the difference ratio between the simulation result and the test result is 8.73% at the maximum and 1.43% at the minimum. The optimal parameter combination obtained by simulation was the rotational speed of 350 r/min, the shelling distance of 5.0 mm, and the filling amount of 40.0%. The results were relatively close, and the difference was within a reasonable range.

ACKNOWLEDGMENTS

The research was supported by China National Natural Science Foundation Project (Grant No. 51457312).

REFERENCES

[1] Baker, A., Dwyer-Joyce, R., Briggs, C., Brockfeld, M. (2012). Effect of different rubber materials on husking dynamics of paddy rice. Proceedings of the Institution of Mechanical Engineers, Part J: *Journal of Engineering Tribology*, Vol.226, Issue 06: 516-528.

[2] Delprete, C., Sesana, R. (2014). Mechanical characterization of kernel and shell of hazelnuts: Proposal of an experimental procedure. *Journal of Food Engineering*, Vol.124, Issue 01: 28-34.

[3] Gao, Y., Song, C., Rao, X., Ying, Y. (2018), Image processing-aided FEA for monitoring dynamic response of potato tubers to impact loading. *Computers and Electronics in Agriculture*, Vol.151:21–30.

[4] Güner M, Dursun E, Dursun İ.G. (2003). Mechanical Behaviour of Hazelnut under Compression Loading. *Biosystems Engineering*, Vol.85, Issue 04: 485-491.

[5] Herak, D., Kabutey, A., Divisova, M., Simanjuntak, S. (2013). Mathematical model of mechanical behaviour of *Jatropha curcas L*. seeds under compression loading. *Biosystems Engineering*, Vol.144, Issue 03:279-288.

[6] Hu, C., Wang, X., Li, H., Wang, L., Li, J., Yang, Y. (2017). Design and test of a new reinforced plastic film collector. *International Agricultural Engineering Journal*, Vol.26, Issue 04: 65-73.

[7] Huang, Z., Cheng, X., Li, C., Xiao, Z., Shi, L (2013). Mechanical model and major influential factors of breaking castor shell. *Journal of Shenyang Agricultural University*, Vol.44, Issue 02: 185-159.

[8] Junming Hou, Zhu Hongjie, Jinpeng Li, Enchao Yao, Hu Weixue. (2020). Analysis and optimization on the process of adjustable double drum castor shelling based on discrete element method, *INMATEH – Agricultural Engineering*, Vol.62, Issue03: 289-298.

[9] Kabutey, A., Herak, D., Chotěborský, R., Dajbych, O., Divišova, M., E. Boatri, W. (2013). Linear pressing analysis of *Jatropha curcas L.* seeds using different pressing vessel diameters and seed pressing heights. *Biosystems Engineering*, Vol.115, Issue 01: 43-49.

[10] Liu, M., Li, C., Zhang, Y., Yang, M., Hou, Y., Gao, L. (2016). Shell crushing mechanism analysis and performance test of flexible-belt shearing extrusion for walnut. T*ransactions of the Chinese Society for Agricultural Machinery*, Vol.47, Issue 07: 267-273.

[11] Liu, R., Cheng, X., Xiao, Z., Li, C., Huang, Z., Ye, H. (2015). Finite element simulation on mechanical property of castor capsule during husking. *Journal of the Chinese Cereals and Oils Association*, Vol.30, Issue 05: 62-66.

[12] Pan, J., Song, W., Liu, H., Shao, N., He, B., Tu, Q. (2019) Research on the Design of Ginkgo Nut Sheller. *Mechanical Engineer*, Vol.01, Issue 04: 92-95.

[13] Rady, A., Soliman, S. (2015). Evaluation of mechanical damage of Lady Rosetta potato tubers using different methods, *International Journal of Postharvest Technology & Innovation*, Vol.05, Issue 02:125-148.

[14] Shi, S., Liu H., Wei, G., Zhou, J., Jian, S., Zhang, R. (2020) Optimization and Experiment of Pneumatic Seed Metering Device with Guided Assistant Filling Based on EDEM-CFD. *Transactions of the Chinese Society for Agricultural Machinery*, Vol.51, Issue 05:54-66.

[15] Wang, L., Quan, Y., Deng, W. (2003). Finite Element Force Analysis of Ginkgo hulling. Journal of Agricultural Engineering, Vol.04, Issue 04: 58-61.

[16] Wang, Z., Xu, J., Li, X., Tian, K., Shen, C. (2015). Mechanical properties test and analysis of Kenaf capsule. *Chinese Journal of agricultural machinery chemistry*, Vol.36, Issue 06: 136-138.

[17] Yuan, Y., Yuan. Y., Dang, X., Xu, Y., Dong, J., Xu, J. (2011). Finite element analysis of mechanical properties of chestnut vacuum cracking. *Journal of Agricultural Machinery*, Vol.42, Issue 05: 136-141.

[18] Zhang, H., Ma, Y., Li, Y., Zhang, R., Zhang, X., Zhang, R. (2014). Prediction model of walnut fracture work based on genetic BP neural network. *Journal of Agricultural Engineering*, 30(18): 78-84.

[19] Zhang, Tao., Liu, F., Zhao, M., Liu, Y., Li, F., Ma, Q., Zhang, Y., Zhou, P. (2017). Measurement of physical parameters of contact between soybean seed and seed metering device and discrete element simulation calibration. *Journal of China Agricultural University*, Vol.22, Issue 09:86-92.

[20] Zhao, Z., Li, Y., Chen, Y., Liang, Z., Liu, L. (2013). Study on the Collision Mechanical properties of rice grains. *Journal of Agricultural Machinery*, Vol.44, Issue 06: 88-92.